



Environmental effects following a seismic sequence: the 2019 Cotabato—Davao del Sur (Philippines) earthquakes

M. F. Ferrario¹ · J. S. Perez² · M. Dizon² · F. Livio¹ · J. Rimando³ · A. M. Michetti^{1,4}

Received: 13 March 2023 / Accepted: 29 January 2024
© The Author(s) 2024

Abstract

In the period of October–December 2019, the Cotabato–Davao del Sur region (Philippines) was hit by a seismic sequence comprising four earthquakes with magnitude $M_W > 6.0$ (EQ1–4; max magnitude M_W 6.8). The earthquakes triggered widespread environmental effects, including landslides and liquefaction features. We documented such effects by means of field surveys, which we supplemented with landslide mapping from satellite images. Field surveys allowed us to gather information on 43 points after EQ1, 202 points after EQs2–3 and 87 points after EQ4. Additionally, we built a multi-temporal inventory of landslides from remote sensing, comprising 190 slope movements triggered by EQ1, 4737 after EQs2–3, and 5666 at the end of the sequence. We assigned an intensity value to each environmental effect using the environmental seismic intensity (ESI-07) scale. Our preferred estimates of ESI-07 epicentral intensity are VIII for the first earthquake and IX at the end of the sequence, which is in broad agreement with other events of similar magnitude globally. This study, which is the first case of the application of the ESI-07 scale to a seismic sequence in the Philippines, shows that repeated documentation of environmental damage and the evaluation of the progression through time may be useful for providing input data for derivative products, such as susceptibility assessment, evaluation of residual risk or investigation of the role played by ground shaking and by other mechanisms able to trigger environmental effects.

Keywords Seismic sequence · Earthquake environmental effects · ESI-07 intensity · Earthquake-induced landslides

✉ M. F. Ferrario
francesca.ferrario@uninsubria.it

¹ Università Degli Studi Dell’Insubria, Como, Italy

² Department of Science and Technology - Philippine Institute of Volcanology and Seismology (DOST-PHIVOLCS), Quezon City, Philippines

³ School of Earth, Environment and Society, McMaster University, 1280 Main Street West, Hamilton, ON L8S 4K1, Canada

⁴ Istituto Nazionale Di Geofisica E Vulcanologia, Sezione Di Napoli Osservatorio Vesuviano, Napoli, Italy

1 Introduction

Seismically active regions are usually exposed to the occurrence of repeated earthquakes over time, which may generate damage to buildings and infrastructures and modify the natural landscape (e.g., Yeats et al. 1996; Michetti et al. 2007; McCalpin 2009; Baker et al. 2021). Commonly, the seismicity pattern comprises a number of foreshocks followed by a mainshock and several aftershocks; the mainshock can be clearly identified given its higher magnitude. Some regions are instead characterized by the occurrence of multiple earthquakes of comparable size in a short time interval (e.g., Hainzl 2004), that we here call seismic sequences. As a matter of fact, seismic sequences produce cumulative effects on the built and natural environment. Documenting the progression of damage through time is thus crucial for disaster risk management purposes, such as for the evaluation of the safety of buildings and infrastructures, eventual evacuation of people at risk, or for identifying safe areas for temporary shelters. On the other hand, assessing the damage evolution due to repeated earthquakes is a challenging task due to time constraints, since the time interval between subsequent earthquakes might be short. Moreover, such a comprehensive assessment requires resources, because the same region should be surveyed multiple times. More commonly, it may not be possible to identify the effects of each seismic event, whereas cumulative effects can be assessed at the end of the sequence (e.g., Graziani et al. 2019; Rossi et al. 2019). Additionally, besides earthquakes, other non-seismic phenomena may occur concurrently and cause additional overprint effects, such as heavy rainfall, in a so-called chain of hazards (e.g., Fan et al. 2019).

In this study, we analyze the seismic sequence that hit the Cotabato—Davao del Sur region (Philippines) in the period of October–December 2019, focusing on the earthquake environmental effects (EEEs). The documentation of EEEs offers a valuable tool to depict the progressive and cumulative damage during seismic sequences because the local geological and geomorphological setting is stable at the timescale of a seismic sequence. Moreover, at high-intensity degrees, macroseismic scales mainly based on the damage to the built environment tend to saturate, while the dimension and amount of EEEs scale with intensity till the highest values (Michetti et al. 2007).

The aims of our work are: (i) to document EEEs triggered by the Cotabato—Davao del Sur seismic sequence through field surveys and remote mapping; (ii) to categorize EEEs using the environmental seismic intensity (ESI-07) scale, which is a macroseismic scale based only on effects on the natural environment (Michetti et al. 2007; Serva et al. 2016; Ferrario et al. 2022); (iii) to evaluate the progression of damage through time, by associating each EEE to its causative event, whenever possible.

The obtained results include two inventories of EEEs mapped during the sequence and one inventory at the end of the sequence; the role of additional concurrent factors (e.g., rainfall) is discussed as well. The multi-temporal assessment of environmental effects during a seismic sequence may be useful to develop time-dependent susceptibility evaluations and to investigate the legacy of repeated ground shaking in the evolution of the erosion and sedimentation processes on a local scale.

2 Regional setting

The tectonic setting of the Philippine archipelago is the result of a complex history. The dominant seismotectonic structures in the region are two oppositely verging subduction zones: To the west, the Philippine Sea Plate (PSP) subducts beneath the Sunda Plate at

a rate of about 7–9 cm/year, whereas, to the east, the Sunda Plate (SP) subducts beneath the Philippines at a rate of about 1 cm/year (Bautista et al. 2001). Here, oblique plate convergence is accommodated by different structures (Fig. 1a): the boundary-perpendicular component is taken up by subduction zones and by strike-slip and thrust/reverse faults in the intervening crustal blocks (Rimando and Rimando 2020; Rimando et al. 2019, 2020, 2022; Perez and Tsutsumi 2017; Marfito et al. 2022). The boundary-parallel component is mainly accommodated by the Philippine Fault Zone (PFZ; Allen 1962; Barrier et al. 1991; Besana and Ando 2005; Nakata et al. 1996; Rimando and Rimando 2020; Perez and Tsutsumi 2017; Tsutsumi and Perez 2013). The PFZ is a major NW–SE oriented left-lateral fault system; in its entirety, it is ~1400 km long and runs almost parallel to the Philippine trench. It comprises creeping sections (e.g., creep rates of ~33 mm/year were documented in the northern and central Leyte sections: Tsutsumi et al. 2016; Fukushima et al. 2019; Dianala et al. 2020) and locked sections. In the southern part, PFZ runs through Mindanao Island (Fig. 1a).

Mindanao is the second largest island of the archipelago and lies at the SE end of the Philippine archipelago. The western part of Mindanao is characterized by the Cotabato

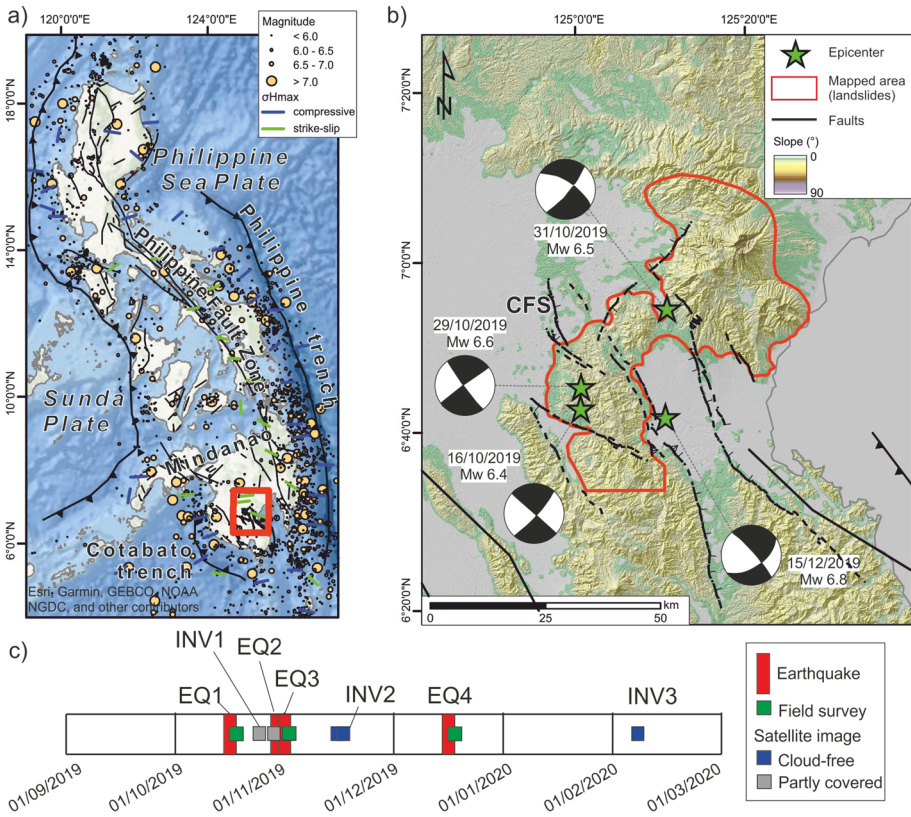


Fig. 1 Tectonic setting of the study area. **a** sketch of the regional seismotectonic setting and historical seismicity, σ Hmax after Heidbach et al. (2018); **b** epicenter of the $M_w > 6.0$ events and mapped area (in red, i.e., the region where landslides have been mapped from satellite images); CFS: Cotabato fault system. Digital surface model AW3D30 (Jaxa) and derived slope map are shown in the background; **c** timeline showing the dates of analyzed satellite images and earthquakes (EQ: earthquake; INV: landslide inventory)

Basin and by the presence of several active faults. Among these, the Cotabato fault system is responsible for the earthquake sequence analyzed in this study. It includes several active faults that are mainly arranged in two orthogonal systems (NW–SE and NE–SW oriented); the present-day strike-slip movement postdates a collisional phase (Pubellier et al. 1994; Quebral et al. 1996). Seismicity in the Philippine archipelago is widespread due to the presence of numerous tectonic elements of major relevance. Figure 1a shows historical seismicity from the ISC catalogue (International Seismological Center 2022); several $M_w > 7$ earthquakes are documented in the region, including the 1879 Surigao earthquake, which generated more than 100 km of surface faulting along the PFZ in Mindanao (Perez and Tsutsumi 2017).

3 The 2019 seismic sequence

In October–December 2019, the Cotabato and Davao del Sur Provinces (Philippines) were hit by four (4) $M_w > 6.0$ earthquakes (maximum M_w 6.8; Fig. 1). The sequence started with a M_w 6.4 on 16 October (EQ1), then three (3) earthquakes with M_w of 6.6, 6.5 and 6.8 occurred on 29 October (EQ2), 31 October (EQ3) and 15 December 2019 (EQ4), respectively. Hypocentral depths range between 10 and 22 km and focal mechanisms indicate strike-slip kinematics (Perez et al. 2020); the position of the events is shown in Fig. 1, while Table 1 provides the main parameters of the four earthquakes.

The source models and slip distribution obtained from inverted InSAR data (Li et al. 2020; Zhao et al. 2021) point to the rupture of two conjugate fault systems during the sequence. EQ1 ruptured a nearly vertical, NW–SE striking, left-lateral fault, resulting in a maximum deformation of ca. 5 cm in the Line of Sight (LOS) direction. EQ2 and EQ3 were modeled together, given the short time interval among them; both the events are related to steep NE–SW striking right-lateral faults, with opposite dip-directions: The seismic source of EQ2 dips toward the NW, whereas the EQ3 source dips to the SW (Li et al. 2020).

Finally, EQ4 is due to a NW–SE striking left-lateral fault and reached a maximum displacement of 30 cm in the LOS direction. Coulomb failure function modeling suggests that the earlier events transferred stress on receiving faults, having a role in promoting the following earthquakes, which indeed occurred in regions with positive stress changes (Li et al. 2020; Zhao et al. 2021).

Table 1 summary of the main seismological parameters of the seismic events. Data from USGS (see data availability section) and Li et al. 2020

ID	Date	Lon (°E)	Lat (°N)	M_w	Strike— RHR (°)	Dip (°)	Rake (°)	Depth (km)
1	16/10/2019	125.007	6.715	6.4	303	86	9	16
2	29/10/2019	125.008	6.757	6.6	234	88	-176	15
3	31/10/2019	125.178	6.910	6.5	036	71	177	10
4	15/12/2019	125.174	6.697	6.8	319	82	-34	22

4 Methods

In order to document the location and dimensions of EEEs, we applied a twofold approach, namely field surveys and mapping from satellite images. In the following, we delineate the methodological aspects belonging to each approach, while in the discussions and interpretations, we provide the complete picture obtained by merging the results. In the following, we define as “mapped area” the region where we perform a systematic mapping of slope movements from satellite images; such area was delineated considering the local morphological setting, i.e., the hilly and mountainous region (Fig. 1b). Instead, we use the term “study area” referring to the region covered either by field surveys or mapping from satellite imagery; the study area covers also the flat regions surrounding the “mapped area.”

4.1 Field surveys

Immediately after each earthquake, the Department of Science and Technology—Philippine Institute of Volcanology and Seismology Quick Response Team (DOST-PHIVOLCS QRT), was deployed in the affected areas to document and investigate the impact of the earthquake. Three batches of the DOST-PHIVOLCS QRT were sent to the affected area, less than two days after the events on October 18, 2019, October 29, 2019, and December 16, 2019, respectively. Geologic impacts attributed to the earthquake sequence include shallow-seated landslides and tension cracks documented around the epicentral and mountainous areas of Tuluhan, Makilala and Kidapawan City in Cotabato Province, Magsaysay, Bansalan and Matanao in Davao del Sur Province and Columbio in Sultan Kudarat Province. Documented EEEs include earthquake-induced landslides, tension cracks and liquefaction or lateral spreading phenomena. The location of each EEEs was retrieved using commercial GPS; a description of the environmental effects and photographic documentation was obtained for over 100 sites (Perez et al. 2019, 2020). In the field, quantitative measures were taken of the elements useful to define the local ESI-07 intensity (see Sect. 4.3). Besides the documentation of EEEs, the surveys were aimed at evaluating areas at risk, focusing in particular on the rapid assessment of the safety of the local population. One of the goals of field surveys was to identify stable and unstable areas, in the framework of evacuation and/or relocation procedures.

4.2 Landslide inventory from satellite images

We map earthquake-triggered landslides from PlanetScope images (orthorectified 4-band multispectral images with 3 m resolution). We aim to attribute as many landslides as possible to their causative earthquake throughout the sequence. We tackle this issue by exploiting PlanetScope images, which have a high temporal resolution (i.e., daily revisit time); nevertheless, the realization of a comprehensive inventory depends on the availability of cloud-free images. Figure 1c shows the timeline of the images used to map the landslides: following EQ1, only a partial inventory (INV1 in the following) could be realized, due to persistent cloud cover. A complete inventory over the mapped area (INV2) is realized on images acquired on November 15 and November 16, 2019, thus encompassing EQ1, EQ2 and EQ3; a third inventory (INV3) is realized on images acquired on February 5, 2020, thus representing the cumulative effect of the entire sequence.

The mapped area (red polygon in Fig. 1) lies between latitude 124°50′–125°30′E and longitude 6°30′–7°10′ N, for a total of 1710 km². We delineate the mapped area by

selecting only areas above a slope threshold of 5° , to reasonably include only slope movements in the obtained inventory, masking out flat regions where liquefaction phenomena could be expected.

Landslides were digitized in a GIS environment based on visual inspection of pre- and post-event satellite images. Pre-event imagery acquired in September 2019 was used to avoid the inclusion of pre-existing landslides in our inventories. Landslides were identified based on the differences in color and texture and delineated as polygons encompassing the whole slope movement (i.e., source areas were not separated from the landslide body; Malamud et al. 2004; Harp et al. 2011). The area of each polygon was calculated in a GIS system. Then, we subdivided the territory into a grid of 1-km^2 cells and we computed the number of landslides (LND, landslide number density) and areal coverage (LAP, landslide areal percentage) for each cell.

4.3 ESI-07 intensity assignment

The assessment of ESI-07 intensity is based on different hierarchical levels: each point where an EEE has been documented is referred to as a “site” and original data should be compiled at this level. Then, sites sharing a homogeneous setting can be grouped into “localities” (Michetti et al. 2004, 2007; Serva et al. 2016). Additionally, the epicentral ESI-07 intensity can be assigned based on the dimension of the area affected by secondary effects, or on the length of surface faulting. Most of the earthquakes analyzed using the ESI-07 scale follow this procedure (Ferrario et al. 2022).

During the field surveys, measured elements at each site were evaluated in order to delineate the ESI-07 local intensity: In the case of liquefaction, such elements include the dimension of sand volcanoes and the length of sand boils alignment; for ground cracks, the width and length was measured; for slope movements, the volume was visually assessed. We remark that the ESI-07 intensity is a classification of environmental effects and that their dimension scales with the intensity degree (Michetti et al. 2007; Serva et al. 2016): As an example, for liquefaction features, ESI-07 intensity VII corresponds to sand boils up to 50 cm in diameter; ESI-07 VIII corresponds to sand boils up to 1 m; ESI-07 intensity IX corresponds to sand boils up to 3 m. Such a kind of quantitative estimation is available for all the types of environmental effects and moving from a given intensity degree to the higher one requires a significant change in the size of the effect.

Beside assigning an ESI-07 value to each site, a grid approach can be also pursued: Here, the territory is divided into regular cells and an ESI-07 value is assigned to each cell. This approach is adopted more rarely (e.g., Ota et al. 2009; Silva et al. 2013) and usually whenever a systematic mapping is realized, such as for landslide inventories. In the case of slope movements, the ESI-07 degree is assigned based on the volume of mobilized material (Michetti et al. 2004); it must be noticed that above 10^6 m^3 an ESI-07 value $\geq X$ can be assigned, i.e., it is not possible to assign ESI-07 XI and XII based on the volume of mobilized material. We obtain the area of each mapped polygon from the GIS system, then an area–volume equation has to be applied, selecting the most suitable among those existing in the literature (Guzzetti et al. 2009; Fan et al. 2019; Yunus et al. 2023). The equation has the general form:

$$V = \alpha \cdot A_i^\gamma \quad (1)$$

where V is the volume in m^3 , A_i is the area of landslide i in m^2 , α and γ are fitting coefficients. Here we adopted the values of Larsen et al. (2010), i.e., $\alpha=0.146$ and $\gamma=1.332$. The selected equation derives from a dataset of over 4000 landslides on a global scale

encompassing either soils or bedrock. The choice of a given equation affects the volume estimation and thus reliable estimates are fundamental for a proper calibration of mitigation strategies (see, e.g., Yunus et al. 2023 for the 2018 Hokkaido-Iburi earthquake). Nevertheless, such uncertainty is of lesser importance for the ESI-07 assessment, since intensity classes are defined on categories spanning different orders of magnitude: For instance, ESI-07 intensity VII corresponds to 10^3 – 10^4 m³, while ESI-07 intensity VIII corresponds to 10^4 – 10^5 m³. In this sense, uncertainty in the delineation of the landslide polygons (e.g., mapping from different authors, amalgamation of multiple source areas in a single polygon) has a stronger effect than the choice of the area–volume equation (Ferrario 2022).

In this paper, we adopt the “site-locality” approach for the points surveyed in the field; for the landslide inventories, we applied the grid approach, which gives more detailed information on the spatial distribution of EEEs. As a last step, and to compare the ESI-07 macroseismic field to other intensity estimates, we manually draw isoseismal lines. We claim that both field surveys and mapping from satellite images provide useful and significant data: Indeed, the two approaches may be seen as somehow complementary in terms of spatial coverage and resolution: Field surveys provide a very accurate description of environmental effects at selected sites, while mapping from satellite imagery allows to obtain a homogeneous inventory over the territory, even in areas difficult to access.

4.4 Comparison with other macroseismic data

Besides the ESI-07 assessment performed in this study, we retrieved information on earthquake damage from PHIVOLCS reports and online questionnaires. PHIVOLCS reports include maps expressed in terms of PEIS (PHIVOLCS Earthquake Intensity Scale), the macroseismic scale adopted in the Philippines since 1996 (Lasala et al. 2015). PEIS intensity is structured in ten degrees, so it differs from other scales which usually have twelve degrees. Damage to buildings starts to appear at PEIS intensity VI; at intensity VII, liquefaction, landslides and damage even to well-built structures are common (Lasala et al. 2015).

We integrated PEIS data with information collected by USGS through the “Did You Feel It” (DYFI) program: Reports from eyewitnesses that compiled an online questionnaire are translated into an intensity measure, expressed using the community decimal intensity (CDI) scale. CDI values are derived to be consistent with the modified Mercalli scale (Wald et al. 2011), with the notable exception of being a decimal value, while all the other intensity scales are ordinal measures.

It is thus clear that ESI-07, PEIS and CDI estimates are not fully comparable with each other: They have different structures (ordinal vs decimal values; ten vs twelve degrees) and focus on different aspects of damage (ESI-07: environmental effects; PEIS: built and natural environment; CDI: felt reports). For this reason, we provide a qualitative comparison, considering maximum values and the spatial pattern of earthquake damage during the entire seismic sequence.

5 Results: distribution of EEEs

5.1 Primary effects

Primary effects include surface faulting and permanent ground deformation. Zhao et al. (2021) inferred from InSAR analysis that slip may have reached the surface following

EQ3; nevertheless, no unequivocal evidence of surface faulting was observed in the field throughout the seismic sequence. Permanent ground deformation is nowadays easily observed through InSAR investigations; deformation lobes were observed for all the events belonging to the Cotabato–Davao del Sur sequence, with maximum deformation values of about 40 cm in the LOS (line of sight) direction (Li et al. 2020; Zhao et al. 2021).

5.2 Secondary effects

We document secondary effects using field surveys and mapping from satellite imagery. Field data provide more detailed information, but at selected sites; remote data were used to map co-seismic landslides and allow to obtain a homogeneous inventory over a wide region. Following EQ1, 43 points were surveyed in the field, while 202 and 87 points are available for EQ2-3 and EQ4, respectively, for a total of 332 observation points (Perez et al. 2019, 2020). Some locations were surveyed multiple times during the seismic sequence, mainly to re-assess the stability of the site and safety for the local population. Figure 2 presents some representative photographs of the type of effects triggered by the earthquakes: Fig. 2a shows an example of numerous shallow-seated landslides in the highly vegetated mountain ranges of Cotabato and Davao del Sur. This aerial photo was taken two days after EQ3 and landslides are still observable as far as the end of photograph. Figure 2b–d presents complex scarps related to slope movements and/or ground cracks observed following EQ1 (Fig. 2b) and EQ3 (Fig. 2c, d). Finally, Fig. 2e shows an example of a liquefaction effect, comprising sand boils and ejected water and sand, observed after EQ3. Most of the points surveyed in the field pertain to slope movements (51% of the total), followed by ground cracks (24%) and liquefaction (22%). Liquefaction was more widespread following EQ4 because its epicenter is in a flat region (Fig. 1b) more susceptible to such phenomena.

5.2.1 Landslide inventories

The availability of high-resolution satellite images with a very short revisit period provides an unprecedented opportunity for constraining the time of occurrence of each slope movement, and for delineating the evolution in time of slope movements with respect to the migration of earthquake epicenters. We realized three inventories:

- *Inventory 1*: landslides triggered by EQ1. Post-event images acquired on 24 and 28/10/2019 were used; cloud-free images cover only 38% of the study area (Fig. 3a). This inventory contains 190 landslides.
- *Inventory 2*: landslides triggered by EQ1, 2 and 3. Satellite images acquired on 15 and 16/11/2019 were used. Landslides were mapped over the entire area and the inventory contains 4737 landslides.
- *Inventory 3*: landslides triggered by EQ1, 2, 3 and 4. Satellite images acquired on 05/02/2020 were used. Landslides were mapped over the entire area and the inventory contains 5666 landslides.

Figure 3 shows the geographical distribution of mapped landslides (inventory 3), while Table 2 provides some figures on the three inventories. Summing the areas of individual landslides, a total of 10.88 km² is reached, corresponding to 0.6% of the mapped area. The



Fig. 2 **a** Aerial shot of numerous shallow-seated landslides documented in the mountain ranges of Cotabato taken two days (02 November 2019) after the EQ3. Take note that landslides are still visible as far as the end of the photograph; **b** complex landslide scarps documented after the EQ1; **c**, **d** ground cracks observed after the EQ3; **e** liquefaction features observed after the EQ3

average area of individual landslides is ca. 2000 m². Figure 3b shows the area–frequency distribution of the landslides, computed following Malamud et al. (2004); inventories 2 and 3 cover the entire mapped area, while inventory 1 represents a much smaller area, due to cloud cover and thus it is to be intended as incomplete. Typically, landslide inventories have a negative power-law distribution for large landslides and a positive power-law distribution for small landslides, separated by a rollover point that represents the modal average of the dataset. For the Cotabato—Davao del Sur datasets, the rollover of inventories 2 and 3 is ca. 600 m², in agreement with existing inventories (e.g., Tanyaş and Lombardo 2020). The exponent of power-law scaling for large landslides (i.e., the slope of the area–frequency distribution) is -2.21 for inventory 2 and -2.67 for inventory 3, in broad agreement with previous studies (e.g., van der Eeckhaut et al. 2007 indicates a value of

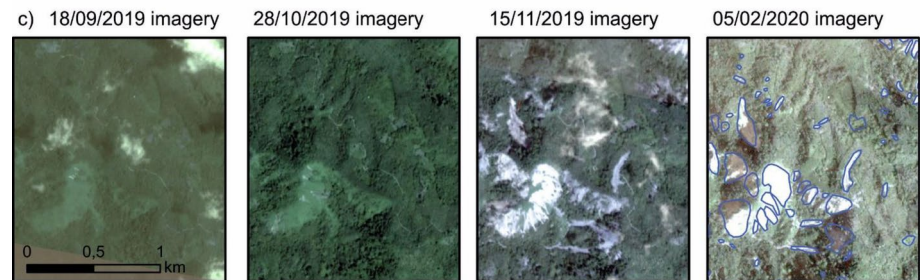
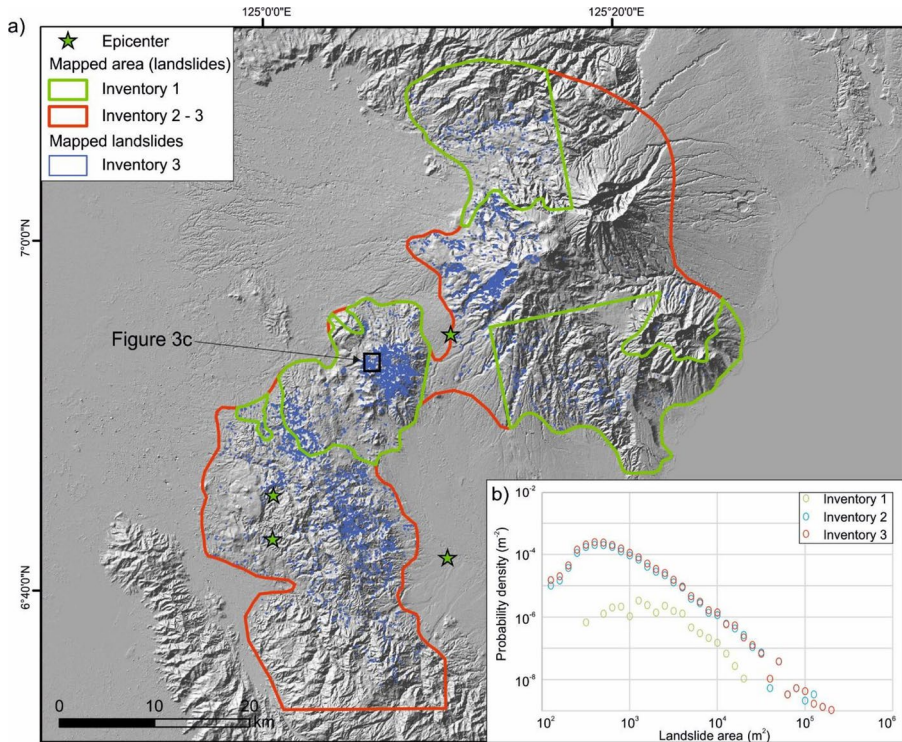


Fig. 3 Multi-temporal images used for this study. **a** final inventory map, showing the landslides triggered by the entire sequence. Red and green polygons outline the area where landslides have been mapped from satellite imagery for the different earthquakes; **b** frequency–magnitude curve obtained for the three inventories; **c** example of pre- and post-event PlanetScope imagery in a heavily affected region, location is shown in panel a. The first image to the left was acquired on 18/09/2019 (before the earthquakes), second image on 28/10 (after EQ1, images used to build inventory 1), the third on 15/11 (after EQs 2–3, images used to build inventory 2), the fourth image on 05/02/2020 (after EQ4, images used to build inventory 3)

Table 2 summary of the characteristics of the 3 landslide inventories

Inventory	Number of landslides	Investigated area (km ²)	Total landslide area (km ²)	Average landslide area (m ²)
1	190	653	0.6	3175
2	4737	1710	9.77	2062
3	5666	1710	10.88	1920

– 2.3 ± 0.6). Three landslides (less than 0.01% of the total landslide population) have volumes higher than 10^6 m^3 , corresponding to ESI-07 values $\geq X$.

Figure 3c shows an example of multi-temporal images in a heavily affected area; at this location, most of the landslides were triggered after 28/10/2019 and before 15/11/2019 (i.e., dates of image acquisition), allowing us to infer EQ2-3 as the causative event.

Figure 4 shows landslide number density (LND) and landslide area percentage (LAP) for the three inventories, calculated on a grid of 1-km^2 cells. Inventory 1 covers a smaller region, due to the lack of cloud-free images; maximum LND and LAP values are 7 landslides/ km^2 and 3%, respectively. Inventories 2 and 3 share the same mapped area, reaching maximum LND and LAP values of 70 landslides/ km^2 and 33%, respectively. The spatial distribution of LND and LAP is fairly similar and higher values concentrate in the central part of the mapped area.

6 Discussion

6.1 Intensity evaluation using the ESI-07 scale

In the ESI-07 framework (Michetti et al. 2007), epicentral intensity can be assessed from the size of primary effects or the dimension of the area affected by secondary effects. Primary effects are absent up to ESI-07 intensity VI; at degree VII, primary effects are observed very rarely and almost exclusively in volcanic areas. Primary effects are observed rarely at intensity ESI-07 VIII and commonly at intensity ESI-07 IX; tectonic subsidence or uplift of the surface reaches maximum values of a few cm for ESI-07 VIII or few dm for ESI-07 IX. For the Cotabato–Davao del Sur sequence, no evidence of surface faulting was observed in the field and permanent ground displacement imaged using InSAR reached a few cm (LOS direction) for EQ1 and a few tens of cm for the other events (Li et al. 2020; Zhao et al. 2021).

The assessment of an ESI-07 value for a slope movement is based on the amount of mobilized volume (in m^3); we measure the area of each mapped landslide and we convert to volume using Eq. (1), adopting the scaling law proposed by Larsen et al. (2010). Recently, Ferrario (2022) investigated the epistemic uncertainty related to the choice of area–volume relations, showing that it does not heavily affect the obtained ESI-07 value, while a much higher influence is due to the quality and reliability of input data (i.e., landslide inventory).

Figure 5 shows the ESI-07 grid maps obtained for the three inventories. For each grid cell, we retain the highest ESI-07 value among the landslides belonging to that cell. Inventory 1 has a maximum ESI-07 value of VIII, while inventories 2 and 3 have a maximum value of $\text{ESI} \geq X$ in the area of Mt. Apo. $\text{ESI-07} \geq X$ is present in only three cells of the study area, which represent 0.15% of the cells (total 1883 cells). The distribution of the ESI-07 values is shown in the histograms of Fig. 5; for all the inventories, most of the cells belong to intensity class VII. In Fig. 5, the right-hand panels show the location of the effects surveyed in the field, color-coded according to their type; it is possible to notice that some points lie outside the area mapped from satellite images, thus providing complementary information which enable to obtain a more complete description of the spatial distribution of secondary effects. Whenever possible, we assign an ESI-07 value to each point based on the dimension of the effect (i.e., heave and length of ground cracks, the volume

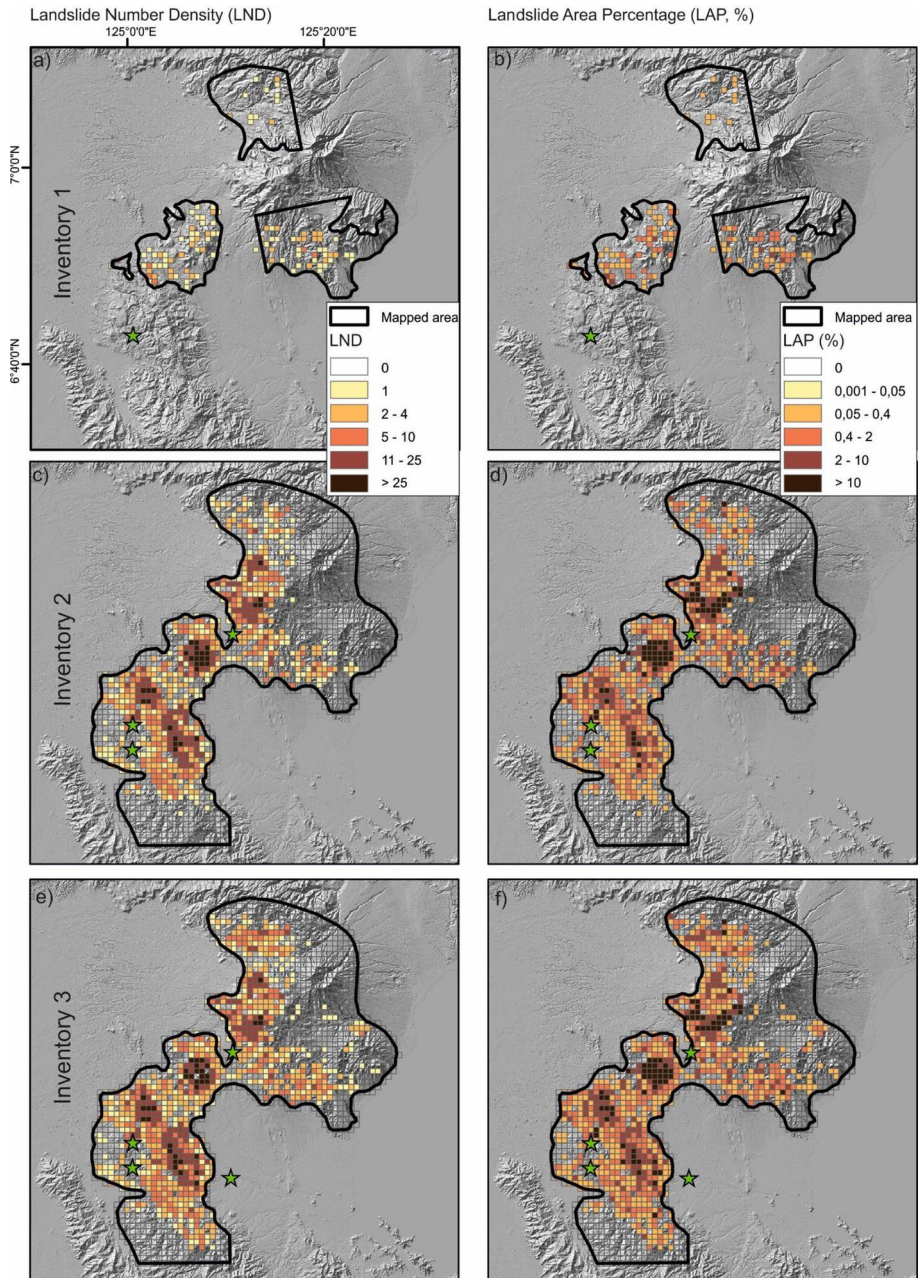


Fig. 4 Landslide density and landslide area percentage for the three inventories. Color scheme after Cramer *et al.* (2020)

of slope movements, diameter of liquefaction sand boils), following the ESI-07 guidelines (Michetti *et al.* 2007).

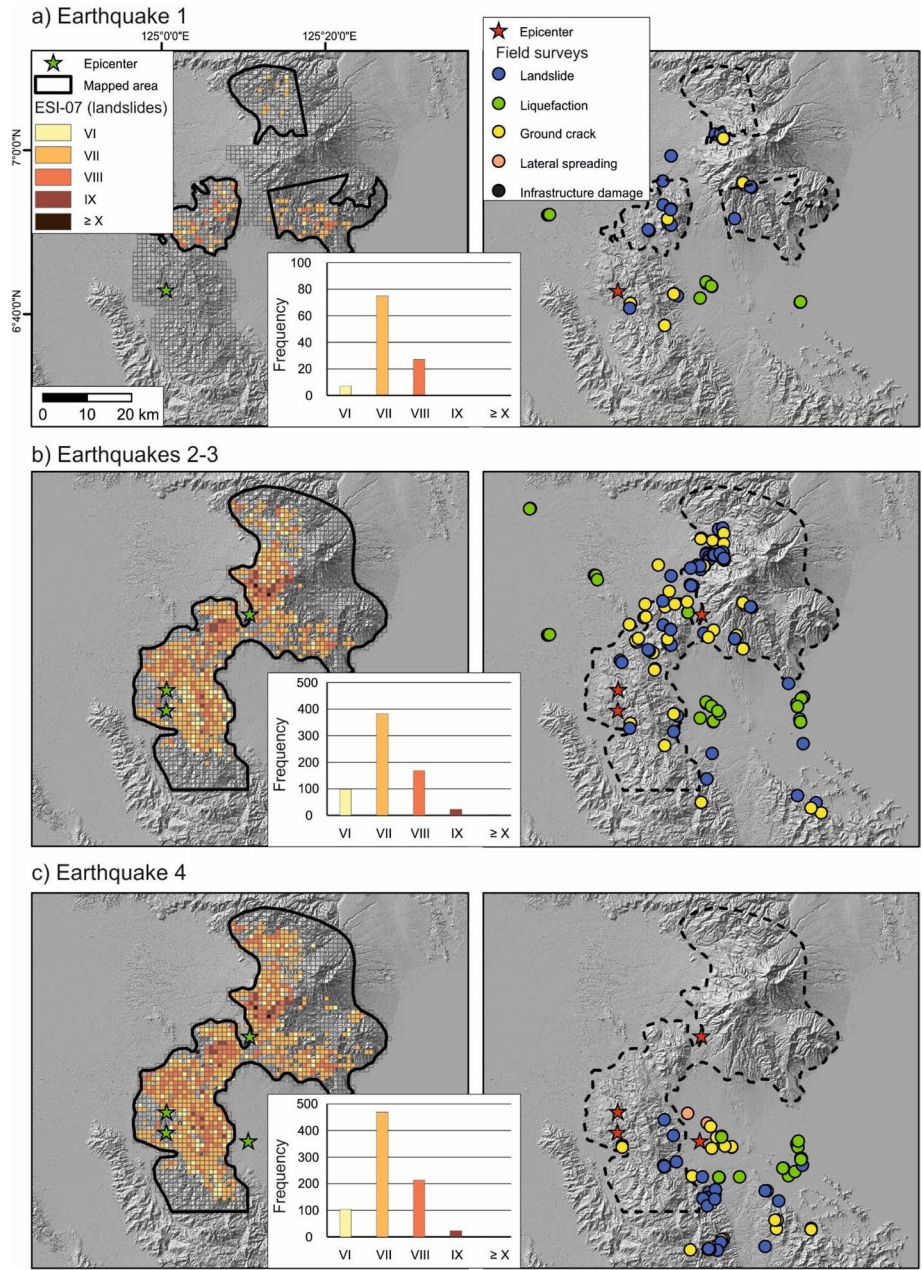


Fig. 5 ESI-07 grid maps (left) and location of points surveyed in the field (right) after EQ1 (a), EQs 1–3 (b) and at the end of the sequence (c); for the left panels, histograms show the ESI-07 distribution of grid cells. Color scheme after Crameri et al. (2020)

The area affected by environmental effects (this study and Perez et al. 2019, 2020) is in the order of 3700 km², which lies between the values corresponding to ESI-07 intensity IX (1000 km²) and ESI-07 X (5000 km²). Considering both primary and secondary effects, our preferred values of ESI-07 epicentral intensity are VIII for EQ1 and IX for EQs 3 and 4; since EQs 2 and 3 occurred only 2 days apart, we are not able to assign an ESI-07 epicentral intensity for EQ2.

6.2 Comparison among intensity measures

In Fig. 6 we provide a summary of the intensity estimates available for the Cotabato–Davao del Sur seismic sequence. The left-hand panels show the isoseismals in terms of the PEIS scale (Perez et al. 2019, 2020), while in the right-hand panels, the ESI-07 isoseismals (this study) are presented together with DYFI data (USGS, see data availability section), expressed as community decimal intensity (CDI). The ESI-07 isoseismals are derived from both field surveys and landslide mapping from satellite images. It is worth recalling that ESI-07 and CDI are 12-degree scales and are built to be consistent with the modified Mercalli (MM) scale, while the PEIS scale has 10 degrees. For this reason, Fig. 6 should be intended in terms of visual comparison among scales, showing the different extent of data availability. Bearing in mind the fundamental differences among intensity scales, only a qualitative comparison can be made; at the bottom of Fig. 6, a conversion table among PEIS and MM intensities is provided, following Besana et al. (1997) and Lasala et al. (2015).

Data for the four earthquakes are summarized in Table 3. EQ1 has lower maximum values than the other earthquakes, regardless of the intensity scale being used. ESI-07 epicentral values are slightly higher than maximum MM values, in good agreement with what has been observed for other case studies (see Ferrario et al. 2022). CDI values peak for EQ2, which seems to contradict the results obtained by other scales; however, the 9.1 value may be an outlier, since the second-most high value is 8.5.

6.3 Moving toward a generalization: comparison with global earthquakes and challenges related to the documentation of seismic sequences

In Fig. 7, we compare the Cotabato–Davao del Sur events with other earthquakes on a global scale (modified after Ferrario 2022). Figure 7a shows the number of landslides with respect to moment magnitude, while Fig. 7b shows the total landslide area (sum of individual landslides); the lines represent the scaling relation proposed by Malamud et al. (2004). The earthquakes analyzed in this study broadly agree with previous data: EQ1 is slightly below the values predicted by Malamud et al. (2004), possibly because the inventory is partial, given the absence of cloud-free images. Instead, earthquakes 2–4 are slightly above expected values, but still close to the data confidence interval. Figure 7c presents the dimension of the area affected by landslides with respect to moment magnitude; open dots include both the events analyzed by Keefer (1984) and more recent data. The Cotabato–Davao del Sur earthquakes are consistent with the values of other case studies available in the literature. Figure 7d shows the comparison with other earthquakes analyzed using the ESI-07 scale (dataset after Ferrario et al. 2022); also in this case the earthquakes analyzed here are in agreement with previous data.

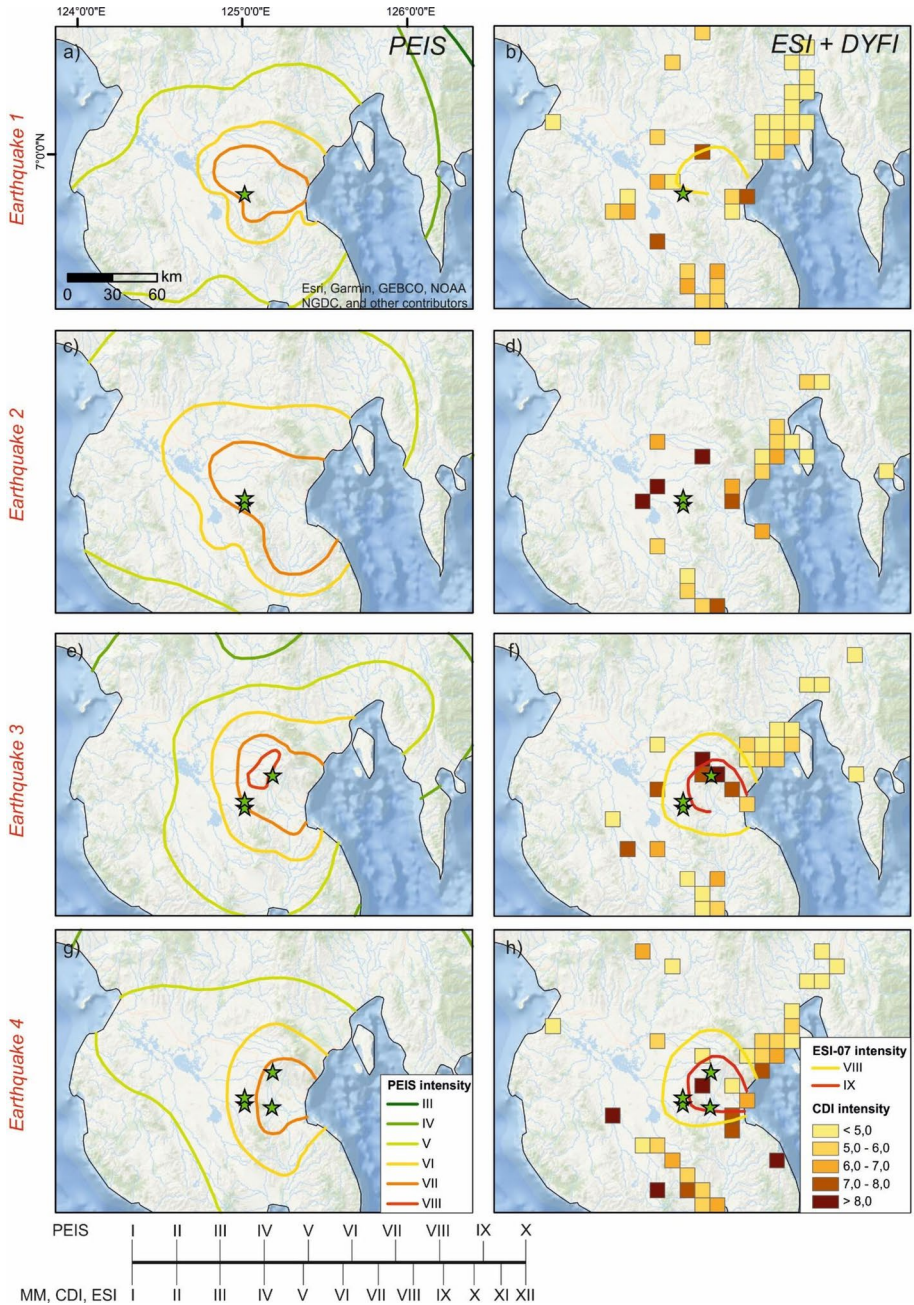


Fig. 6 Summary of intensity estimates for EQ1 (a–b), EQ2 (c–d), EQ3 (e–f) and EQ4 (g–h); left-hand panels show PEIS isoseismals (after Perez et al. 2019, 2020); right-hand panel show ESI-07 isoseismals (this study) and CDI values retrieved from USGS. A conversion table between intensity scales is provided as well (after Lasala et al. 2015)

Table 3 Comparison of the intensity values obtained using different scales, namely the PEIS, MM, CDI and ESI-07 scales. N.a.: not available

	EQ1	EQ2	EQ3	EQ4
Date	16–10-2019	29–10-2019	31–10-2019	15–12-2019
Max PEIS value	VII	VII	VIII	VII
Max MM value	VII	VII	VIII–IX	VII
Max CDI value	7.8	9.1	8.6	8.9
ESI-07 epicentral value	VIII	n.a	IX	IX

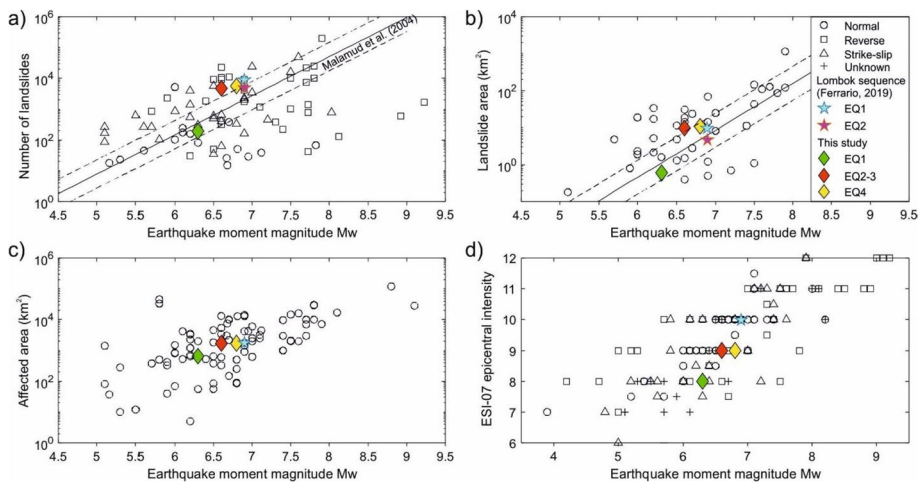


Fig. 7 Comparison of the Cotabato–Davao del Sur sequence with global studies, including the multi-temporal inventory provided by Ferrario (2019) for the Lombok (Indonesia) seismic sequence. **a** the number of landslides vs M_w , regression is after Malamud et al. (2004); **b** landslide area vs M_w , regression is after Malamud et al. (2004); **c** affected area vs M_w ; **d** ESI-07 epicentral intensity vs M_w , dataset is after Ferrario et al. (2022)

6.4 The concurrent role of multiple earthquakes and rainfall

During a seismic sequence, the area is subjected to repeated stresses due to ground shaking generated by each earthquake. Several authors investigated the evolution of EEEs triggered by multiple earthquakes in a short time interval: Quigley et al. (2016) provide a detailed investigation of the 2010–2011 Canterbury (New Zealand) sequence, including evidence for repeated liquefaction at a single place (Quigley et al. 2013). Papathanassiou et al. (2017) analyzed the effects triggered by the January/February 2014 Cephalonia, (Greece) earthquakes. Roback et al. (2018) built an inventory of landslides triggered by a M_w 7.2 earthquake that occurred 3 weeks after the M_w 7.8 mainshock (Gorkha, Nepal). Ferrario (2019) built a multi-temporal inventory for the 2018 Lombok (Indonesia) seismic sequence.

All these studies testify that earthquakes can repeatedly trigger environmental effects at the same place; earthquake damage, and thus macroseismic intensity, can remain constant or increase during a seismic sequence, but it can never decrease. Our results show a worsening in the amount and severity of EEEs during the Cotabato–Davao del Sur sequence,

as testified by the number of landslides, the area affected by secondary effects and derived ESI-07 intensity (Fig. 7). The first earthquake of the sequence had a M_w 6.4, while subsequent events reached a maximum magnitude of M_w 6.8. This can explain the low number of landslides triggered by EQ1: Despite INV1 being incomplete, cloud-free areas clearly show that most of the landslides were triggered by EQs2-4 (e.g., Fig. 3). The epicenters of the 4 earthquakes are about 20 km apart; an increasing crustal volume is thus progressively involved in the sequence, explaining the wider dimension of the area affected by EEEs. Additionally, the epicenter of EQ4 lies in a flat area more prone to liquefaction, as verified in the field.

Another mechanism that commonly triggers environmental effects, especially slope movements, is rainfall. Earthquakes and precipitation may play a concurrent role either in the short term (weeks to months) or in the longer term (Parker et al. 2015; Fan et al. 2018; Marc et al. 2019; Tian et al. 2020). Landslide debris may be remobilized by subsequent rainfall and several studies demonstrated an overall increase in landslide activity following a strong earthquake, which then decreases to pre-earthquake values in several years (e.g., Marc et al. 2015; Chen et al. 2020; Fan et al. 2021). The long-term legacy of earthquakes on the territory can also be traced in the alteration of the sedimentary input into rivers (e.g., Hovius et al. 2011) and in the influence of past earthquakes on the distribution of environmental effects for more recent events (Parker et al. 2015; Tanyaş et al. 2021). Usually, the peak landslide rate is observed in the co-seismic phase (Tanyaş et al. 2021) and the enhanced post-seismic landslide rate may not add significantly to the total mobilized volume: For instance, Marc et al. (2015) estimated the post-seismic volume in 2–5% of the total. Fan et al. (2018) showed that most of the co-seismic debris after the 2008 Wenchuan earthquake was stabilized along the hillslopes and not eroded by rainfall. Additionally, Fan et al. (2021) demonstrated that the prediction capability of seismic-related variables on the pattern of co-seismic landslides decreases with time after an earthquake, while hydrological and topographic parameters show the opposite trend.

When seismic events and heavy precipitation are co-located in time and space, understanding the relative importance of seismic triggers and precipitation is even more complex. The increasing availability of satellite images with a short revisit time (e.g., one or few days as in the case of PlanetScope images) provides the opportunity to build multi-temporal inventories, which aid in identifying the triggering process; nevertheless, cloud cover may remain a problem when analyzing optical imagery. Regarding precipitation data, they are nowadays available in many parts of the world with varying temporal resolution (e.g., the global precipitation measurement (GPM) mission managed by NASA). As an example, we mention the M_w 7.2 earthquake that hit Haiti on 14/08/2021: It was followed by Hurricane Grace only two days later, which produced up to 38 cm of rainfall. Havenith et al. (2022) and Zhao et al. (2022) estimated that co-seismic landslide inventories may be overestimated by about 10–15% due to the effects triggered by Grace, which include the widening of slope failures triggered by the earthquake. Nevertheless, no new landslides have been observed in the cloud-free images acquired immediately before and after hurricane Grace (Havenith et al. 2022).

The Cotabato–Davao del Sur sequence occurred in the rainy season and in order to provide information on the role of rainfall in triggering landslides, we present the daily accumulated precipitation (Huffman et al. 2019) at five periods throughout the seismic sequence in Fig. 8; we also present a time series of the precipitation over the area depicted in the maps. Data are retrieved from the Global Precipitation Measurement Mission managed by NASA (See Data availability section) and are expressed in mm/day, with a resolution of 0.1° ; data were accessed through Giovanni online system (see Data Availability).

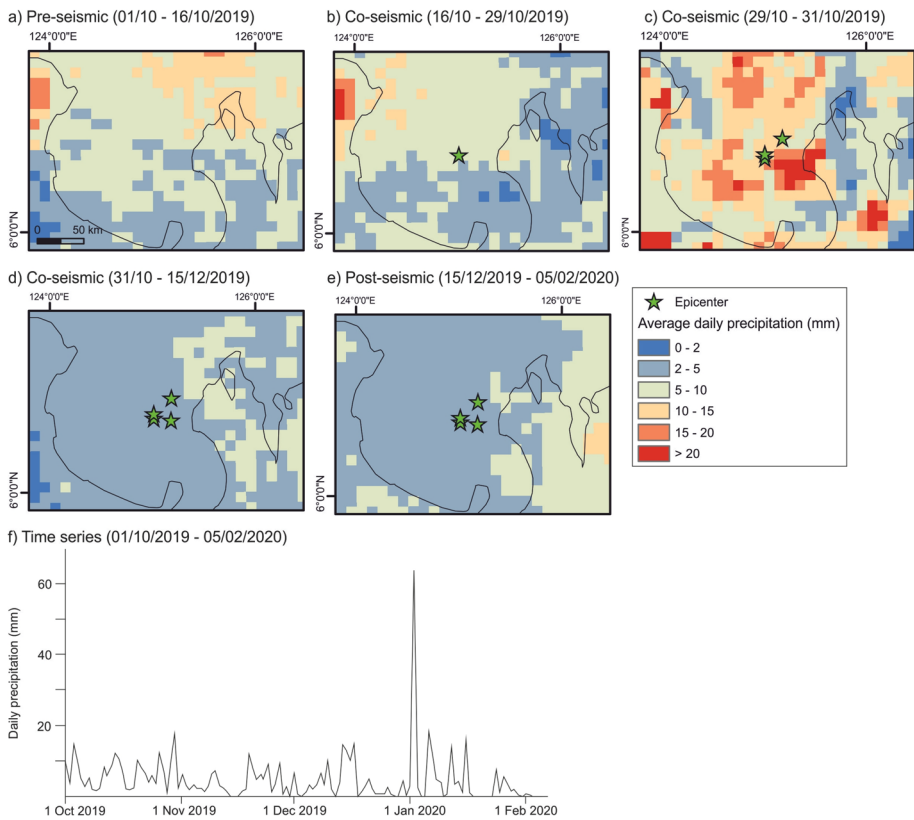


Fig. 8 precipitation data (average daily precipitation in mm, accessed using Giovanni online data system) during several time intervals throughout the seismic sequence; **a** 15-day antecedent precipitation; **b** precipitation after EQ1 and before EQ2; **c** precipitation after EQ2 and before EQ3; **d** precipitation after EQ3 and before EQ4; **e** post-seismic precipitation; **f** time series of the average daily precipitation data, over the area depicted in the maps

Figure 8a shows the average daily precipitation in the 15-day antecedent EQ1 (01/10/2019 to 16/10/2019) highlighting that the study area falls in the average daily precipitation class of 5–10 mm. Figure 8b presents the time interval between 16 and 28/10/2019, with values similar to the pre-seismic phase. Figure 8c highlights heavy rainfall (> 15 mm/day) during 29–31/10/2019, that is between EQ2 and EQ3. In the two months between EQ3 and EQ4 (Fig. 8d) and after the end of the sequence (Fig. 8e) rainfall is much lower (values < 5 mm/day). The time series plot (Fig. 8f) allows to observe a prominent peak on 02/01/2020, with 64 mm of rainfall over the area; however, when averaged over the longer time window (15/12/2019 to 05/02/2020) the daily rainfall is limited.

From the combined analysis of earthquakes and precipitation data, we argue that M_W 6.4 (EQ1) is not high enough to trigger widespread landslides in the study area. EQs2-3 were more efficient in triggering landslides. One reason may be related to seismological factors, namely the higher magnitude and possible weakening of the slopes from previous events; on the other hand, conspicuous rainfall hit the study area on the same days, possibly enhancing the landslide rate. Despite the even higher magnitude of EQ4, the total number of landslides is only 20% higher than that of EQs2-3; possible explanations include the

deeper hypocentral depth or the fact that all the available material has been already mobilized, but more investigations are needed to fully evaluate this issue.

Overall, we claim that the multi-temporal inventory developed in this study may be useful in the analysis of susceptibility to EEEs for subsequent earthquakes over a short-term (e.g., Burrows et al. 2020; Xue et al. 2022) and the mutual role of seismic shaking and rainfall (e.g., Fan et al. 2021; Tanyaş et al. 2021).

7 Conclusions

In this paper, we analyzed earthquake environmental effects (EEEs) triggered by the Cotabato–Davao del Sur seismic sequence, providing the first application of the ESI-07 scale on a seismic sequence in the Philippines; we collected original data directly in the field and we mapped slope movements from satellite images. We compiled a multi-temporal landslide inventory, pertaining to the landslides triggered after Earthquake 1, after Earthquake 3 and after Earthquake 4. The inventories comprise 190, 4737 and 5666 slope movements, respectively. The earthquakes have a similar magnitude (M_w range 6.4–6.8), but we notice that earthquakes 2 and 3 (i.e., landslide inventory 2) were much more effective than Earthquake 4 in triggering slope movements. This observation can be associated with two reasons: Earthquake 4 had a deeper hypocentral depth (22 km vs the 10–16 km of the other events within the sequence) and the epicentral location is more to the East, slightly outside the mountainous region. We did not notice significant differences in terms of characteristics of the individual triggered landslides: The average area is about 2000 m³ for both inventories 2 and 3 (see Table 2) and the spatial distribution of landslide density and areal percentage values is similar.

The ESI-07 epicentral intensity is assessed at VIII for Earthquake 1 and at IX for Earthquakes 3–4. Here we focus on the documentation of earthquake environmental effects and on their interpretation in terms of ESI-07 intensity assessment; we argue that our dataset can be used as an input for obtaining derivative products. For instance, the landslide inventories provide the grounds to proceed to susceptibility mapping: The availability of multi-temporal inventories of environmental effects during seismic sequences is still spare and we believe that the Cotabato–Davao del Sur case history can be used as a reference for realizing similar studies. The realization of multiple field surveys at the same locations throughout the seismic sequence and the short revisit time of satellite images allow to tightly pinpoint the time of occurrence of the mapped effects. Additionally, our landslide inventories are made from manual mapping and can enhance the validation of products obtained through automatic processes. Overall, we highlight that the documentation of environmental damage throughout seismic sequences, and its interpretation in terms of ESI-07 assessment, provides the opportunity to investigate the characteristics of the different fault segments that may be involved in a sequence of earthquakes; future efforts should focus on the mechanisms of chain triggering of repeated earthquakes, which are of clear societal relevance.

Acknowledgements We acknowledge Planet for providing PlanetScope imagery as part of the Education and Research program. We appreciate the help of “Marie Curie” High School (Meda, Italy) students, who assisted in digitizing part of the inventory, in the framework of the national PCTO program (Percorsi per le Competenze Trasversali e per l’Orientamento), under the coordination of Prof. Mariantonia Resnati. The authors would also like to acknowledge all the members of the Department of Science and Technology—Philippine Institute of Volcanology and Seismology Quick Response Team (DOST-PHIVOLCS QRT), who participated in the field investigation of the 2019 Cotabato—Davao del Sur Earthquake Sequence.

Author contributions MFF performed the data conceptualization and methodological ideation. JSP and MD realized the fieldwork. Data collection, formal analysis and investigation was realized by MFF, JSP, FL and JR. The first draft of the manuscript was written by MFF and all authors commented on previous versions of the manuscript. All authors read and approved the final manuscript.

Funding Open access funding provided by Università degli Studi dell'Insubria within the CRUI-CARE Agreement. The authors declare that no funds, grants, or other support were received during the preparation of this manuscript.

Data availability The USGS event pages are accessible from <https://earthquake.usgs.gov/earthquakes/>. Shapefiles of the landslide inventories and the investigated area are available on Zenodo (coordinates WGS84 UTM zone 51N). Files can be downloaded at <https://doi.org/10.5281/zenodo.7520726>. The data used to draw Fig. 7 are available on the Zenodo repository at <https://doi.org/10.5281/zenodo.6107187>. Analyses and visualizations of precipitation data were produced with the Giovanni online data system (<https://giovanni.gsfc.nasa.gov>; last access: November 2023), developed and maintained by the NASA GES DISC. The Integrated Multi-satellitE Retrievals for GPM (IMERG) are available at <https://doi.org/10.5067/GPM/IMERGDF/DAY/06>. ALOS-DEM AW3D30 is provided by JAXA (Japan Aerospace Exploration Agency) and is available at https://www.eorc.jaxa.jp/ALOS/en/dataset/aw3d30/aw3d30_e.htm.

Declaration

Conflict of interest All the authors declare that they have no financial interests.

Open Access This article is licensed under a Creative Commons Attribution 4.0 International License, which permits use, sharing, adaptation, distribution and reproduction in any medium or format, as long as you give appropriate credit to the original author(s) and the source, provide a link to the Creative Commons licence, and indicate if changes were made. The images or other third party material in this article are included in the article's Creative Commons licence, unless indicated otherwise in a credit line to the material. If material is not included in the article's Creative Commons licence and your intended use is not permitted by statutory regulation or exceeds the permitted use, you will need to obtain permission directly from the copyright holder. To view a copy of this licence, visit <http://creativecommons.org/licenses/by/4.0/>.

References

- Allen C (1962) Circum-Pacific faulting in the Philippines-Taiwan region. *J Geophys Res* 67(12):4795–4812. <https://doi.org/10.1029/JZ067i012p04795>
- Baker J, Bradley B, Stafford P (2021) *Seismic hazard and risk analysis*. Cambridge University Press, Cambridge
- Barrier E, Huchon P, Aurelio M (1991) Philippine fault: a key for Philippine kinematics. *Geol* 19:32. [https://doi.org/10.1130/0091-7613\(1991\)019%3c0032:PFAKFP%3e2.3.CO;2](https://doi.org/10.1130/0091-7613(1991)019%3c0032:PFAKFP%3e2.3.CO;2)
- Bautista BC, Bautista MLP, Oike K et al (2001) A new insight on the geometry of subducting slabs in northern Luzon, Philippines. *Tectonophysics* 339:279–310. [https://doi.org/10.1016/S0040-1951\(01\)00120-2](https://doi.org/10.1016/S0040-1951(01)00120-2)
- Besana GM, Ando M (2005) The central Philippine Fault Zone: location of great earthquakes, slow events and creep activity. *Earth Planet Space* 57:987–994. <https://doi.org/10.1186/BF03351877>
- Besana GM, Negishi H, Ando M (1997) The three-dimensional attenuation structures beneath the Philippine archipelago based on seismic intensity data inversion. *Earth Planet Sci Lett* 151:1–11. [https://doi.org/10.1016/S0012-821X\(97\)00112-X](https://doi.org/10.1016/S0012-821X(97)00112-X)
- Burrows K, Walters RJ, Milledge D, Densmore AL (2020) A systematic exploration of satellite radar coherence methods for rapid landslide detection. *Nat Hazards Earth Syst Sci* 20:3197–3214. <https://doi.org/10.5194/nhess-20-3197-2020>
- Chen M, Tang C, Xiong J et al (2020) The long-term evolution of landslide activity near the epicentral area of the 2008 Wenchuan earthquake in China. *Geomorphology* 367:107317. <https://doi.org/10.1016/j.geomorph.2020.107317>
- Cramer F, Shephard GE, Heron PJ (2020) The misuse of colour in science communication. *Nat Commun* 11(1):1–10. <https://doi.org/10.1038/s41467-020-19160-7>

- Dianala JDB, Jolivet R, Thomas MY, Fukushima Y, Parsons B, Walker R (2020) The relationship between seismic and aseismic slip on the Philippine Fault on Leyte Island Bayesian modeling of fault slip and geothermal subsidence. *J Geophys Res* 125(12):e2020JB020052. <https://doi.org/10.1029/2020JB020052>
- Fan X, Scaringi G, Xu Q et al (2018) Coseismic landslides triggered by the 8th August 2017 Ms 7.0 Jiuzhaigou earthquake (Sichuan, China): factors controlling their spatial distribution and implications for the seismogenic blind fault identification. *Landslides* 15:967–983. <https://doi.org/10.1007/s10346-018-0960-x>
- Fan X, Scaringi G, Korup O et al (2019) Earthquake-Induced chains of geologic hazards: patterns, mechanisms, and impacts. *Rev Geophys* 57:421–503. <https://doi.org/10.1029/2018RG000626>
- Fan X, Yunus AP, Scaringi G et al (2021) Rapidly evolving controls of landslides after a strong earthquake and implications for hazard assessments. *Geophys Res Lett*. <https://doi.org/10.1029/2020GL090509>
- Ferrario MF (2019) Landslides triggered by multiple earthquakes: insights from the 2018 Lombok (Indonesia) events. *Nat Hazards* 98:575–592. <https://doi.org/10.1007/s11069-019-03718-w>
- Ferrario MF (2022) Landslides triggered by the 2015 M_w 6.0 Sabah (Malaysia) earthquake: inventory and ESI-07 intensity assignment. *Nat Hazards Earth Syst Sci* 22:3527–3542. <https://doi.org/10.5194/nhess-22-3527-2022>
- Ferrario MF, Livio F, Michetti AM (2022) Fifteen years of environmental seismic intensity (ESI-07) scale: dataset compilation and insights from empirical regressions. *Quatern Int* 625:107–119. <https://doi.org/10.1016/j.quaint.2022.04.011>
- Fukushima Y, Hashimoto M, Miyazawa M et al (2019) Surface creep rate distribution along the Philippine fault, Leyte Island, and possible repeating of $M_w \sim 6.5$ earthquakes on an isolated locked patch. *Earth Planets Space* 71:118. <https://doi.org/10.1186/s40623-019-1096-5>
- Graziani L, del Mese S, Tertulliani A et al (2019) Investigation on damage progression during the 2016–2017 seismic sequence in Central Italy using the European Macroseismic Scale (EMS-98). *Bull Earthq Eng* 17:5535–5558. <https://doi.org/10.1007/s10518-019-00645-w>
- Guzzetti F, Ardizzone F, Cardinali M et al (2009) Landslide volumes and landslide mobilization rates in Umbria, central Italy. *Earth Planet Sci Lett* 279:222–229. <https://doi.org/10.1016/j.epsl.2009.01.005>
- Hainzl S (2004) Seismicity patterns of earthquake swarms due to fluid intrusion and stress triggering. *Geophys J Int* 159(3):1090–1096
- Harp EL, Keefer DK, Sato HP, Yagi H (2011) Landslide inventories: the essential part of seismic landslide hazard analyses. *Eng Geol* 122:9–21. <https://doi.org/10.1016/j.enggeo.2010.06.013>
- Havenith H-B, Guerrier K, Schlögel R et al (2022) Earthquake-induced landslides in Haiti: analysis of seismotectonic and possible climatic influences. *Nat Hazards Earth Syst Sci* 22:3361–3384. <https://doi.org/10.5194/nhess-22-3361-2022>
- Heidbach O, Rajabi M, Cui X, Fuchs K, Müller B, Reinecker J, Reiter K, Tingay M, Wenzel F, Xie F, Ziegler MO, Zoback ML, Zoback MD (2018) The World Stress Map database release 2016: crustal stress pattern across scales. *Tectonophysics* 744:484–498. <https://doi.org/10.1016/j.tecto.2018.07.007>
- Hovius N, Meunier P, Lin C-W et al (2011) Prolonged seismically induced erosion and the mass balance of a large earthquake. *Earth Planet Sci Lett* 304:347–355. <https://doi.org/10.1016/j.epsl.2011.02.005>
- Huffman GJ, Stocker EF, Bolvin DT, Nelkin EJ, Tan J (2019) GPM IMERG final precipitation L3 1 day 0.1 degree x 0.1 degree V06. In: Savtchenko A, Greenbelt MD (eds) Goddard earth sciences data and information services center (GES DISC). Accessed Jan 2023, [10.5067/GPM/IMERGDF/DAY/06](https://doi.org/10.5067/GPM/IMERGDF/DAY/06)
- International Seismological Center (2022) ISC-GEM Earthquake Catalogue, Version 9.0, Accessed January 2023. <https://doi.org/10.31905/d808b825>
- Keefer DK (1984) Landslides caused by earthquakes. *Geol Soc Am Bull* 95(4):406–421
- Larsen IJ, Montgomery DR, Korup O (2010) Landslide erosion controlled by hillslope material. *Nature Geosci* 3:247–251. <https://doi.org/10.1038/ngeo776>
- Lasala M, Inoue H, Tiglao R et al (2015) Establishment of earthquake intensity meter network in the Philippines. *J Disaster Res* 10:43–50. <https://doi.org/10.20965/jdr.2015.p0043>
- Li B, Li Y, Jiang W et al (2020) Conjugate ruptures and seismotectonic implications of the 2019 Mindanao earthquake sequence inferred from Sentinel-1 InSAR data. *Int J Appl Earth Obs Geoinf* 90:102127. <https://doi.org/10.1016/j.jag.2020.102127>
- Malamud BD, Turcotte DL, Guzzetti F, Reichenbach P (2004) Landslides, earthquakes, and erosion. *Earth Planet Sci Lett* 229:45–59. <https://doi.org/10.1016/j.epsl.2004.10.018>
- Marc O, Hovius N, Meunier P et al (2015) Transient changes of landslide rates after earthquakes. *Geology* 43:883–886. <https://doi.org/10.1130/G36961.1>
- Marc O, Behling R, Andermann C et al (2019) Long-term erosion of the Nepal Himalayas by bedrock landsliding: the role of monsoons, earthquakes and giant landslides. *Earth Surf Dyn* 7:107–128. <https://doi.org/10.5194/esurf-7-107-2019>

- Marfito BJ, Llamas DCE, Aurelio MA (2022) Geometry and segmentation of the Philippine fault in Surigao strait. *Front Earth Sci* 10:799803. <https://doi.org/10.3389/feart.2022.799803>
- McCalpin J (2009) *Paleoseismology*. Academic Press, Cambridge
- Michetti AM, Esposito E, Gurpinar A et al (2004) (2004) The INQUA Scale. An innovative approach for assessing earthquake intensities based on seismically-induced ground effects in natural environment. In: Vittori E, Comerci V (eds) *Memorie Descrittive della Carta Geologica d'Italia*, vol 67. APAT, Rome, pp 1–118
- Michetti AM, Esposito E, Guerrieri L et al (2007) Environmental seismic intensity scale-ESI 2007, *Memorie descrittive della carta geologica d'Italia*, 74, 41 pp., ISBN 978–88–240–2903–2, Accessed January 2023 <https://www.isprambiente.gov.it/en/publications/technical-periodicals/descriptive-memories-of-the-geological-map-of-intensity-scale-esi-2007>
- Nakata T, Tsutsumi H, Punongbayan R, et al (1996) Surface fault ruptures of the 1990 Luzon earthquake, Philippines, Special Publication 25. Research Center for Regional Geography, Hiroshima University, Hiroshima, Japan
- Ota Y, Azuma T, Lin YN (2009) Application of INQUA environmental seismic intensity scale to recent earthquakes in Japan and Taiwan. *SP* 316:55–71. <https://doi.org/10.1144/SP316.4>
- Papathanassiou G, Valkaniotis S, Ganas A (2017) Evaluation of the macroseismic intensities triggered by the January/February 2014 Cephalonia, (Greece) earthquakes based on ESI-07 scale and their comparison to 1867 historical event. *Quatern Int* 451:234–247. <https://doi.org/10.1016/j.quaint.2016.09.039>
- Parker RN, Hancox GT, Petley DN et al (2015) Spatial distributions of earthquake-induced landslides and hillslope preconditioning in the northwest South Island, New Zealand. *Earth Surf Dyn* 3:501–525. <https://doi.org/10.5194/esurf-3-501-2015>
- Perez JS, Abigania MI, Abitang MF et al. (2019) The October 2019 Cotabato earthquake sequence: parameters and impacts. *GeoCon 2019: Geoscience for a resilient and sustainable Philippines*. December 4–5, 2019, Manila Hotel, Manila, Philippines. Accessed January 2023. https://www.researchgate.net/publication/341368489_The_October_2019_Cotabato_earthquake_sequence_Parameters_and_impacts
- Perez J, Amilbahar RG, Baltazar HM et al (2020) Fault geometry and geologic impacts of the 15 December 2019 magnitude 6.9 Davao del Sur earthquake. *Virtual Geocon 2020, 75 Years of Geosciences in the Philippines: opportunities, advances, and frontiers*. Accessed January 2023. https://www.researchgate.net/publication/346648501_Fault_Geometry_and_Geologic_Impacts_of_the_15_December_2019_Magnitude_6.9_Davao_del_Sur_Earthquake
- Perez JS, Tsutsumi H (2017) Tectonic geomorphology and paleoseismology of the Surigao segment of the Philippine fault in northeastern Mindanao Island, Philippines. *Tectonophysics* 699:244–257. <https://doi.org/10.1016/j.tecto.2017.02.001>
- Pubellier M, Deffontaines B, Quebral R, Rangin C (1994) Drainage network analysis and tectonics of Mindanao, southern Philippines. *Geomorphology* 9:325–342. [https://doi.org/10.1016/0169-555X\(94\)90053-1](https://doi.org/10.1016/0169-555X(94)90053-1)
- Quebral RD, Pubellier M, Rangin C (1996) The onset of movement on the Philippine fault in eastern Mindanao: a transition from a collision to a strike-slip environment. *Tectonics* 15:713–726. <https://doi.org/10.1029/95TC00480>
- Quigley MC, Bastin S, Bradley BA (2013) Recurrent liquefaction in Christchurch, New Zealand, during the Canterbury earthquake sequence. *Geology* 41(4):419–422
- Quigley MC, Hughes MW, Bradley BA et al (2016) The 2010–2011 Canterbury earthquake sequence: environmental effects, seismic triggering thresholds and geologic legacy. *Tectonophysics* 672–673:228–274. <https://doi.org/10.1016/j.tecto.2016.01.044>
- Rimando R, Rimando J (2020) Morphotectonic kinematic indicators along the Vigan–Aggao Fault—the western deformation front of the Philippine Fault Zone in Northern Luzon. *Philipp Geosci* 10(2):83. <https://doi.org/10.3390/geosciences10020083>
- Rimando J, Aurelio M, Dianala JD et al (2019) Coseismic ground rupture of the October 15, 2013 Magnitude (M_w) 7.2 Bohol earthquake, Bohol Island. *Central Philipp Tecton* 38:2558–2580. <https://doi.org/10.1029/2019TC005503>
- Rimando R, Rimando J, Lim R (2020) Complex shear partitioning involving the 6 February 2012 MW 6.7 Negros earthquake ground rupture in central Philippines. *Geosciences* 10(11):460. <https://doi.org/10.3390/geosciences10110460>
- Rimando J, Williamson A, Mendoza RB, Hobbs T (2022) Source model and characteristics of the 27 July 2022 MW 7.0 Northwestern Luzon earthquake. *Seismica, Philippines*. <https://doi.org/10.26443/seismica.v1i1.217>

- Roback K, Clark MK, West AJ et al (2018) The size, distribution, and mobility of landslides caused by the 2015 Mw7.8 Gorkha earthquake. *Nepal Geomorphol* 301:121–138. <https://doi.org/10.1016/j.geomorph.2017.01.030>
- Rossi A, Tertulliani A, Azzaro R et al (2019) The 2016–2017 earthquake sequence in Central Italy: macroseismic survey and damage scenario through the EMS-98 intensity assessment. *Bull Earthq Eng* 17:2407–2431. <https://doi.org/10.1007/s10518-019-00556-w>
- Serva L, Vittori E, Comerci V et al (2016) Earthquake hazard and the environmental seismic intensity (ESI) scale. *Pure Appl Geophys* 173:1479–1515. <https://doi.org/10.1007/s00024-015-1177-8>
- Silva PG, Pérez-Lopez R, Rodríguez-Pascua MA et al. (2013) Earthquake environmental effects (EEEs) triggered by the 2011 Lorca Earthquake (Mw 5.2, Betic Cordillera, SE Spain): application of the ESI-07 Macroseismic Scale. 4th INQUA PATA meeting, Aachen, Germany
- Tanyaş H, Lombardo L (2020) Completeness Index for earthquake-induced landslide inventories. *Eng Geol* 264:105331. <https://doi.org/10.1016/j.enggeo.2019.105331>
- Tanyaş H, Kirschbaum D, Lombardo L (2021) Capturing the footprints of ground motion in the spatial distribution of rainfall-induced landslides. *Bull Eng Geol Environ* 80:4323–4345. <https://doi.org/10.1007/s10064-021-02238-x>
- Tian Y, Owen LA, Xu C et al (2020) Landslide development within 3 years after the 2015 Mw 7.8 Gorkha earthquake. *Nepal Landslides* 17:1251–1267. <https://doi.org/10.1007/s10346-020-01366-x>
- Tsutsumi H, Perez JS (2013) Large-scale active fault map of the Philippine fault based on aerial photograph interpretation. *Act Fault Res*. https://doi.org/10.11462/afr.2013.39_29
- Tsutsumi H, Perez JS, Lienkaemper, JJ (2016) Variation of surface creep rate along the Philippine fault based on surveys of alignment arrays and offset cultural features. AGU Fall Meeting Abstracts. <https://ui.adsabs.harvard.edu/abs/2016AGUFM.T23A2907T/abstract>
- van der Eeckhaut M, Poesen J, Govers G, Verstraeten G, Demoulin A (2007) Characteristics of the size distribution of recent and historical landslides in a populated hilly region. *Earth Planet Sci Lett* 256(2007):588–603
- Wald DJ, Quitariano V, Worden CB, Hopper M, Dewey JW (2011). USGS “Did You Feel It?” Internet-based macroseismic intensity maps. *Ann Geophys*, 54(6).
- Xue C, Chen K, Tang H, Lin C, Cui W (2022) Using short-interval landslide inventories to build short-term and overall spatial prediction models for earthquake-triggered landslides based on machine learning for the 2018 Lombok earthquake sequence. *Nat Hazards* 114(3):3575–3595
- Yeats RS, Sieh K, Allen CR (1996) *The geology of earthquakes*. Oxford University Press, Oxford
- Yunus AP, Xinyu C, Catani F, Subramaniam SS, Fan X, Jie D, Sajinkumar KS, Gupta A, Avtar R (2023) Earthquake-induced soil landslides: volume estimates and uncertainties with the existing scaling exponents. *Sci Rep* 13(1):8151
- Zhao L, Qu C, Shan X et al (2021) Coseismic deformation and multi-fault slip model of the 2019 Mindanao earthquake sequence derived from Sentinel-1 and ALOS-2 data. *Tectonophysics* 799:228707. <https://doi.org/10.1016/j.tecto.2020.228707>
- Zhao B, Wang Y, Li W et al (2022) Evaluation of factors controlling the spatial and size distributions of landslides, 2021 Nippes earthquake. *Haiti Geomorphol* 415:108419. <https://doi.org/10.1016/j.geomorph.2022.108419>